

Optical Extinction Predictions from Measurements on the Open Sea

G. L. TRUSTY and T. H. COSDEN

*Optical Radiation Branch
Optical Sciences Division*

January 19, 1979



NAVAL RESEARCH LABORATORY
Washington, D.C.

Approved for public release; distribution unlimited.

SECURITY CLASSIFICATION OF THIS PAGE (When Data Entered)

REPORT DOCUMENTATION PAGE		READ INSTRUCTIONS BEFORE COMPLETING FORM
1. REPORT NUMBER NRL Report 8260	2. GOVT ACCESSION NO.	3. RECIPIENT'S CATALOG NUMBER
4. TITLE (and Subtitle) OPTICAL EXTINCTION PREDICTIONS FROM MEASUREMENTS ON THE OPEN SEA		5. TYPE OF REPORT & PERIOD COVERED Interim report on a continuing NRL problem.
		6. PERFORMING ORG. REPORT NUMBER
7. AUTHOR(s) G.L. Trusty and T. H. Cosden		8. CONTRACT OR GRANT NUMBER(s)
9. PERFORMING ORGANIZATION NAME AND ADDRESS Naval Research Laboratory Washington, D.C. 20375		10. PROGRAM ELEMENT, PROJECT, TASK AREA & WORK UNIT NUMBERS NRL Problem R05-31 PE 63745N; Task S-0182-AA
11. CONTROLLING OFFICE NAME AND ADDRESS Naval Sea Systems Command Washington, D.C. 20362		12. REPORT DATE January 19, 1979
		13. NUMBER OF PAGES 25
14. MONITORING AGENCY NAME & ADDRESS (if different from Controlling Office)		15. SECURITY CLASS. (of this report) UNCLASSIFIED
		15a. DECLASSIFICATION/DOWNGRADING SCHEDULE
16. DISTRIBUTION STATEMENT (of this Report) Approved for public release; distribution unlimited.		
17. DISTRIBUTION STATEMENT (of the abstract entered in Block 20, if different from Report)		
18. SUPPLEMENTARY NOTES		
19. KEY WORDS (Continue on reverse side if necessary and identify by block number) Aerosols Marine Maritime Optical transmission		
20. ABSTRACT (Continue on reverse side if necessary and identify by block number) From aerosol measurements made aboard a ship in the open sea, we calculated extinction coefficients at several optical wavelengths, using the size distribution and Mie theory. We made the measurements at points along a path from the coast of Virginia to Rota, Spain, then into the Mediterranean to Greece. Most of the measurements were made under moderate to high visibility conditions, but fog was encountered once. The measurements are limited by ship influences.		

CONTENTS

INTRODUCTION	1
EQUIPMENT	2
PARTICLE COUNTER CALIBRATION.....	5
EQUIPMENT PLACEMENT.....	5
MEASUREMENTS	6
MARITIME AEROSOL MODELS.....	9
COMPUTATIONAL APPROACH.....	15
SUMMARY.....	17
REFERENCES	18
APPENDIX — Aerosol Data	19

OPTICAL EXTINCTION PREDICTIONS FROM MEASUREMENTS ON THE OPEN SEA

INTRODUCTION

In the spring of 1977, USNS *Hayes* (Fig. 1), research vessel of the Naval Research Laboratory (NRL), crossed the Atlantic from Virginia to Spain, then continued into the Mediterranean as far as Greece. The purpose of the cruise was to make micrometeorological and optical measurements of the atmosphere on the open sea. The experiments were designed in particular to measure aerosol size distributions to be used for calculating extinction coefficients as a function of wavelength.

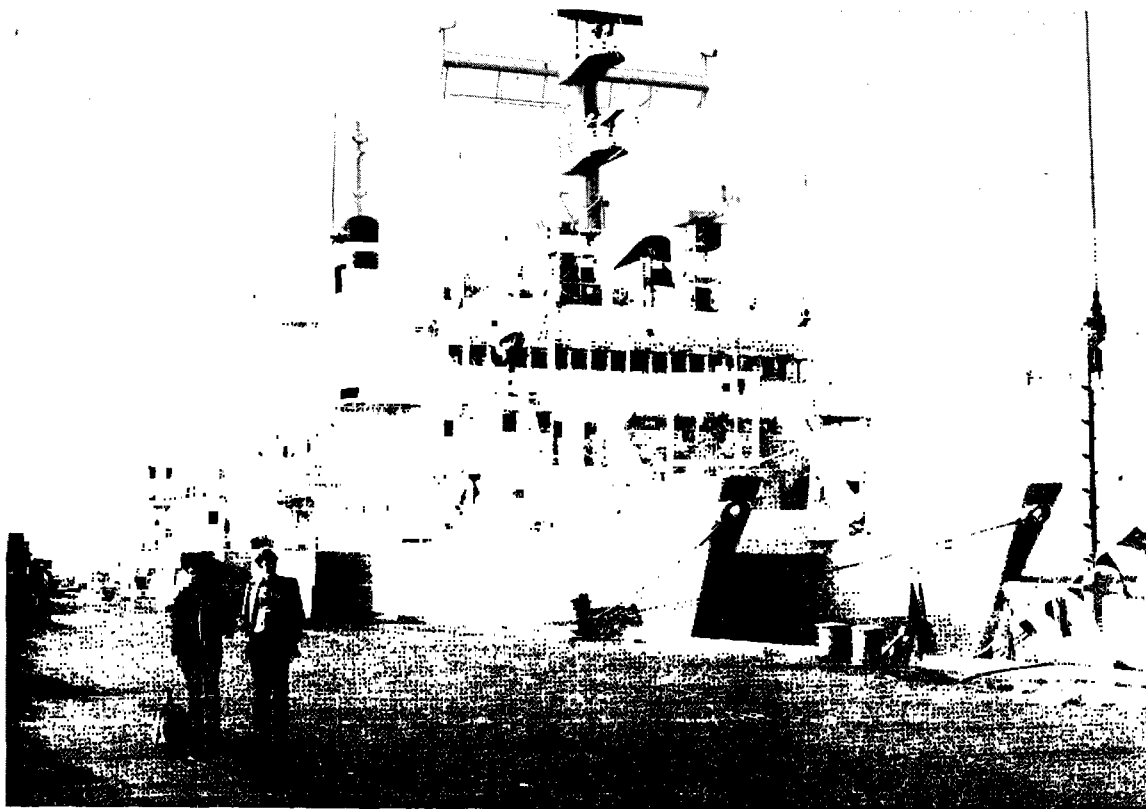


Fig. 1 — USNS *Hayes*, showing locations of particle spectrometers (squares)

EQUIPMENT

Particle Measuring Systems, Inc. (PMS) particle spectrometers* were placed in two locations to measure aerosol size distributions. One probe sat near the starboard bow, about 9 m from the ocean surface. Two were just forward of the bridge at a height of about 15 m. The squares in Fig. 1 show the locations.

These probes normally function on land as part of the mobile laboratory shown schematically in Fig. 2, which indicates two primary sets of sensors. The meteorological set on the upper left includes devices for monitoring air temperature, dewpoint, windspeed, and wind direction. On the upper right are two particle spectrometers. One is an Active Aerosol Spectrometer Probe (ASASP) which measures particles with radii in the 0.1- to 2.0- μm range. The second is a high-volume scattering probe (CSASP), which covers a range of 1.0 to 15 μm . The electronics that handle the data from the sensors are in the mobile laboratory and are illustrated in three columns in Fig. 2. The center column shows the

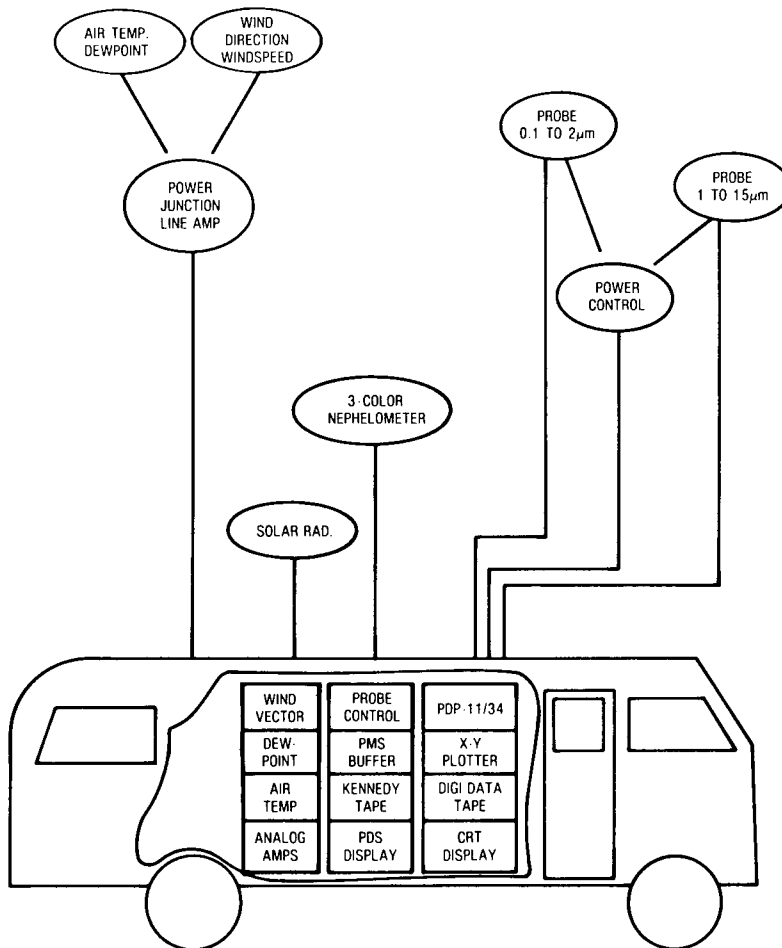


Fig. 2 — Mobile laboratory as usually operated

*Particle Measuring Systems, 1855 South 57th Court, Boulder, CO 80301.

PMS electronics, which include the data buffer and a digital magnetic tape where the information from all sensors is stored every second.

Simultaneously, the system feeds the information into the PDP-11/34 Data Acquisition System for real-time processing. The user may specify averaging times. Data reduction includes the generation of aerosol size distributions from the probe data and the calculation, from these distributions, of extinction coefficients for five arbitrary wavelengths by the Mie scattering theory. A disk stores resultant extinction coefficients, size distributions, and averaged meteorological parameters at the end of each averaging period. These data later produce time plots or cross-correlation plots. A three-color nephelometer was used, but the wet, salt-laden atmosphere rendered it useless, so this report does not discuss the nephelometer results.

Figure 3 shows an expanded version of the measurement system. A second high-volume particle spectrometer and another set of meteorological instruments recently have been added for use as a remote station. However, for use on the ship, a short cable replaced the microwave link. Note that the data from both stations go through the PMS data buffer onto the Kennedy tape, so that simultaneous information from both sites can be compared.

To the left of the PDP-11/34 in Fig. 3 is a terminal that converses with the CPU. Figure 4 gives an example of real-time output on that terminal, from the computer program used on Hayes' cruise. The top line shows the year, day, time of day, and length of the averaging time. The next line of numbers gives the air temperature, dewpoint, windspeed, wind direc-

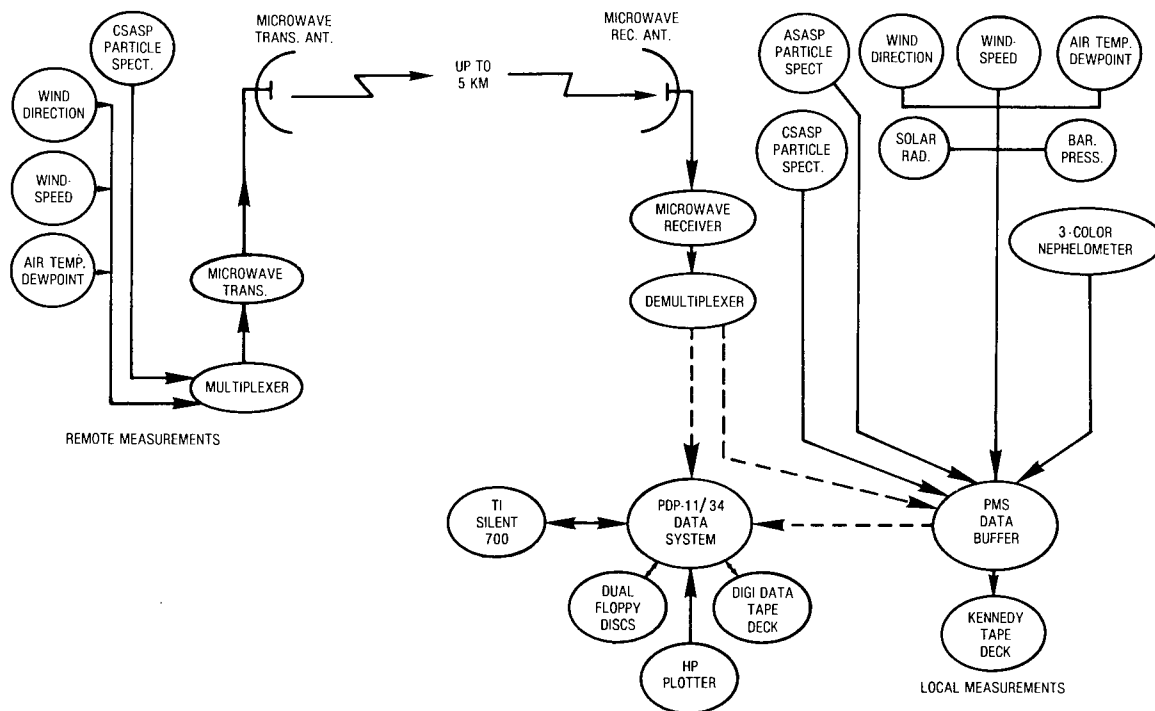


Fig. 3 — Aerosol measurement system

TRUSTY AND COSDEN

77:147:1533 MINAVG=30

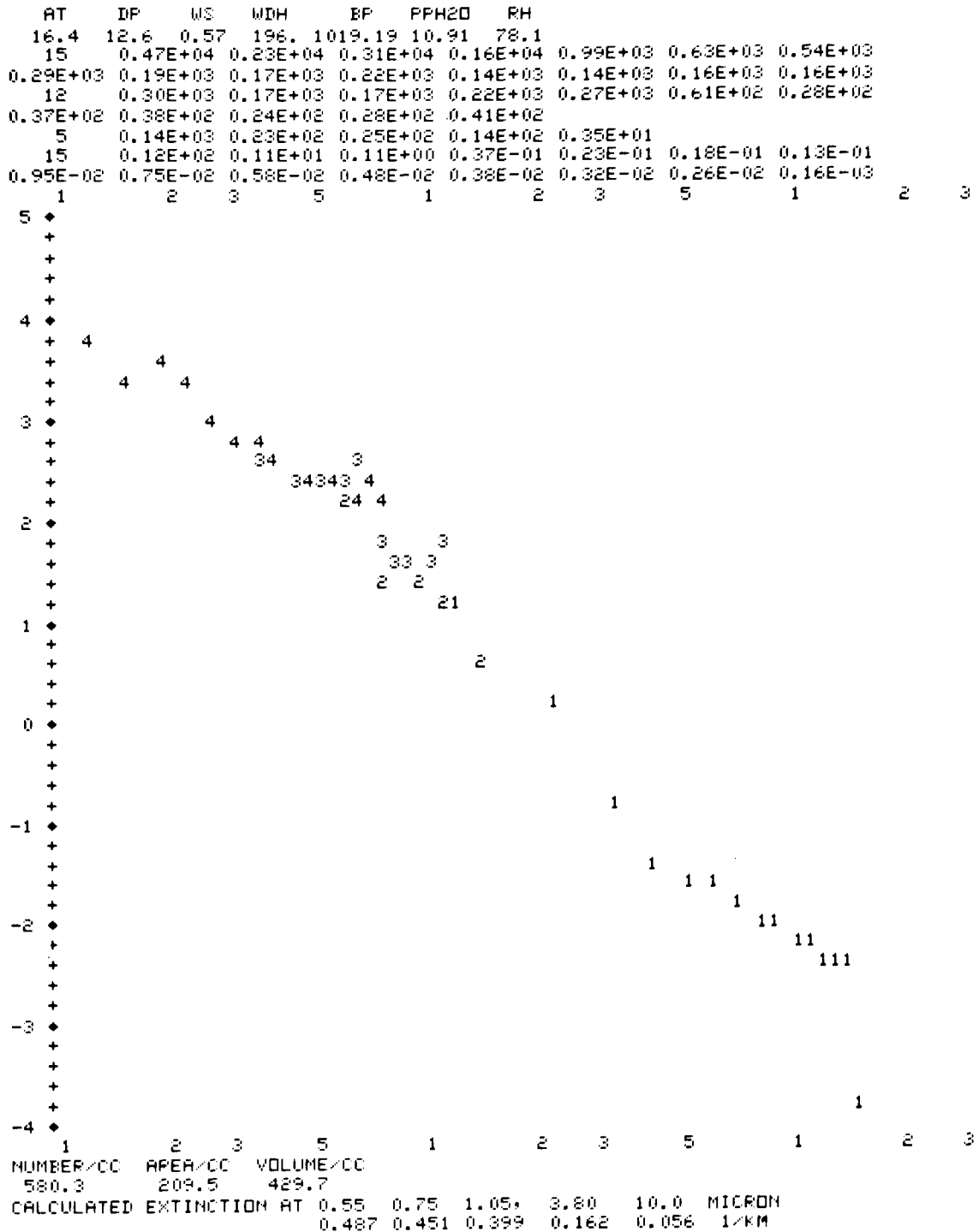


Fig. 4 — Sample real-time output from the data acquisition system

tion, barometric pressure, partial pressure of water vapor (calculated from the dewpoint), and the relative humidity (from the dewpoint and air temperature). The next series gives the values of the points plotted on the particle size distribution below the numbers. The plot is dN/dR ($\text{cm}^{-3} \mu\text{m}^{-1}$), where N is the particle concentration and R is the particle radius, versus R (μm) in a log-log form, with the vertical scale covering a range of 10^{-4} to 10^{+5} as shown, and the horizontal scale covering a range of 0.1 to 30. On the curve itself, the numbers 4, 3, and 2 indicate the three ranges of the active scattering probe, and a 1 indicates results from the high-volume scattering probe.

The on-line program uses the distribution to calculate, in real time, the particle number density (cm^{-3}), the cross-sectional area density ($\mu\text{m}^2 \text{cm}^{-3}$), and the volume density ($\mu\text{m}^3 \text{cm}^{-3}$). The results of those calculations appear directly beneath the plot. Finally, from the distribution, the extinction coefficients (per kilometer) at five wavelengths (micrometers indicated as microns) are calculated in real time, as shown in the last line. These extinction coefficients, obtained from Mie theory, give only the extinction due to the aerosols; no molecular absorption or Rayleigh scattering is included.

PARTICLE COUNTER CALIBRATION

Although calibration equipment is taken into the field in case of emergency, we rely on the manufacturer's calibration of the aerosol probes. The instruments are calibrated before each major field trip. If it seems warranted, the calibration is repeated after the trip. Calibration is done using glass beads for the larger size ranges and polystyrene or latex spheres for the smaller sizes. Adjustment is seldom needed during calibrations.

The manufacturer gives an accuracy of 10% to the flow rates and plus or minus one sampling bin size for particle sizing. The error in the flow rate converts directly with respect to an extinction coefficient calculation. The bin-size error is more complex. Due to the steep slope on many of the size distributions, a one-bin displacement may not appear to change the curve much, but a calculation of extinction coefficients may reveal an order-of-magnitude effect.

Nevertheless, we have made several comparisons [1,2] with other instruments running concurrently and have found agreement generally better than the one-bin error would predict. Further, we have measured particles at sites in conjunction with optical transmission measurements. When wind direction and relative humidity were taken into account, predicted and measured transmissions compared favorably.

EQUIPMENT PLACEMENT

Due to size and shipping requirements, we had to remove the main electronic modules from the mobile laboratory and place them in a container (Fig. 5). The air conditioner on the roof was needed to reduce the relative humidity to the point at which the computer disks would function properly.

Figures 6 and 7 show the locations of the three PMS probes and the meteorological sensors. The active probe and one of the high-volume probes are seen in Fig. 6 at their locations forward of the bridge on the starboard side. Figure 6 also shows, above the bridge, many instruments of other scientists on the cruise. Figure 7, a view from above the bridge

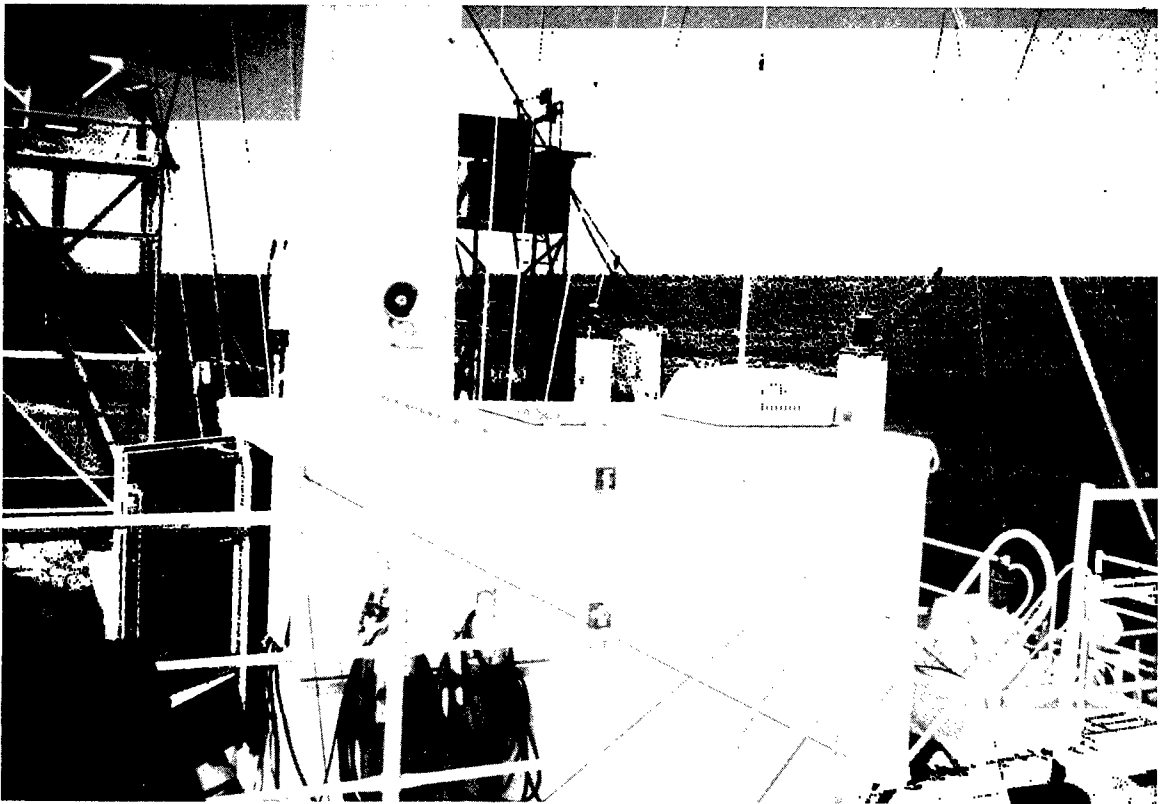


Fig. 5 — Equipment enclosure used aboard ship

down to the starboard bow, shows the location of the second high-volume probe. The meteorological sensors are clearly visible in this figure. The bottom right of the photograph shows the edge and horn of the active probe and indicates the relative location of the two sets of instruments.

Because of the large and high superstructures on the ship, instruments have to be located carefully to avoid turbulent eddies that might modify the air sample. In Fig. 8, the airflow is being checked at the entrance of the pair of probes just forward of the bridge. The laminar flow pattern indicates that there is little ship influence at this point. Similar tests showed the flow at the bow probe to be acceptable also.

MEASUREMENTS

Figure 9 illustrates the ship's path on the cruise. The plus signs indicate 1200Z on successive days. The small circles indicate times when the measurements were representative of a marine atmosphere alone. The problem is illustrated in Fig. 10, which shows the effluent from the ship's stack on the horizon. Measurements of the marine atmosphere taken aboard a ship demand great care, to prevent taking measurements of the ship's atmosphere. In fact, since most of the crossing on this cruise involved a following wind, reliable marine atmosphere

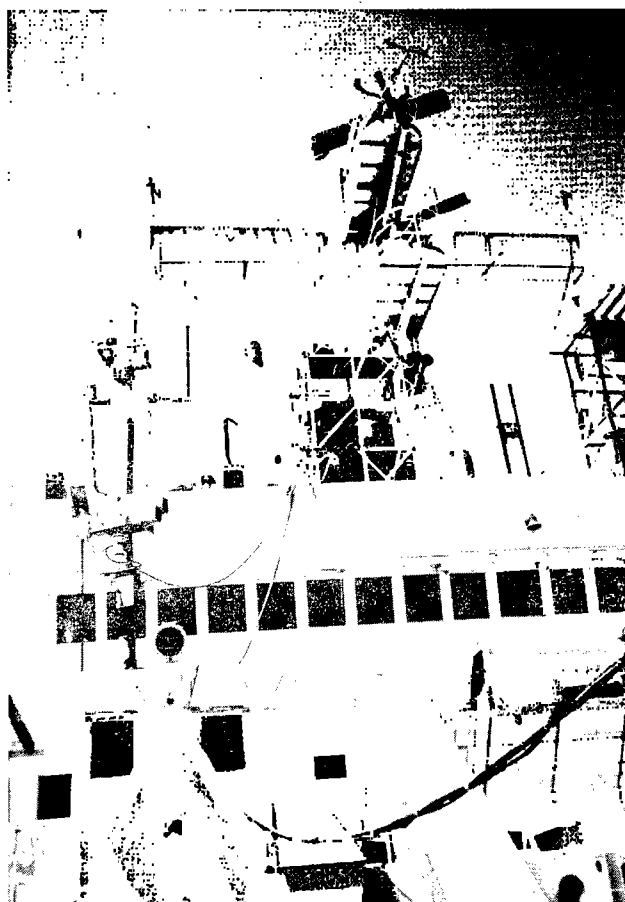


Fig. 6 — View of bridge, showing equipment location (square)

measurements required that the ship stop and turn into the wind. The circles in Fig. 9 indicate each of these periods, generally of an hour's duration.

An example of the severity of this ship influence is shown in Fig. 11. This shows two aerosol size distributions; one with the wind from the stern while the ship was under way, and one with the wind from the bow after the ship had stopped and turned into the wind. There is an enormous difference. For present purposes, however, the important result is the effect of the change in distributions on the calculated extinction coefficients. Figure 12 is a plot of extinction coefficient vs wavelength for the two cases. With a stern wind, the result is at best inadequate for any type of optical performance prediction.

This example leads to two conclusions. First, proper sampling techniques are imperative. Second, achieving this state of technology may be very difficult if the sensors are limited to onboard measurements. For example, our solution to the sampling problem — turning the ship around — would be unacceptable under operational conditions.

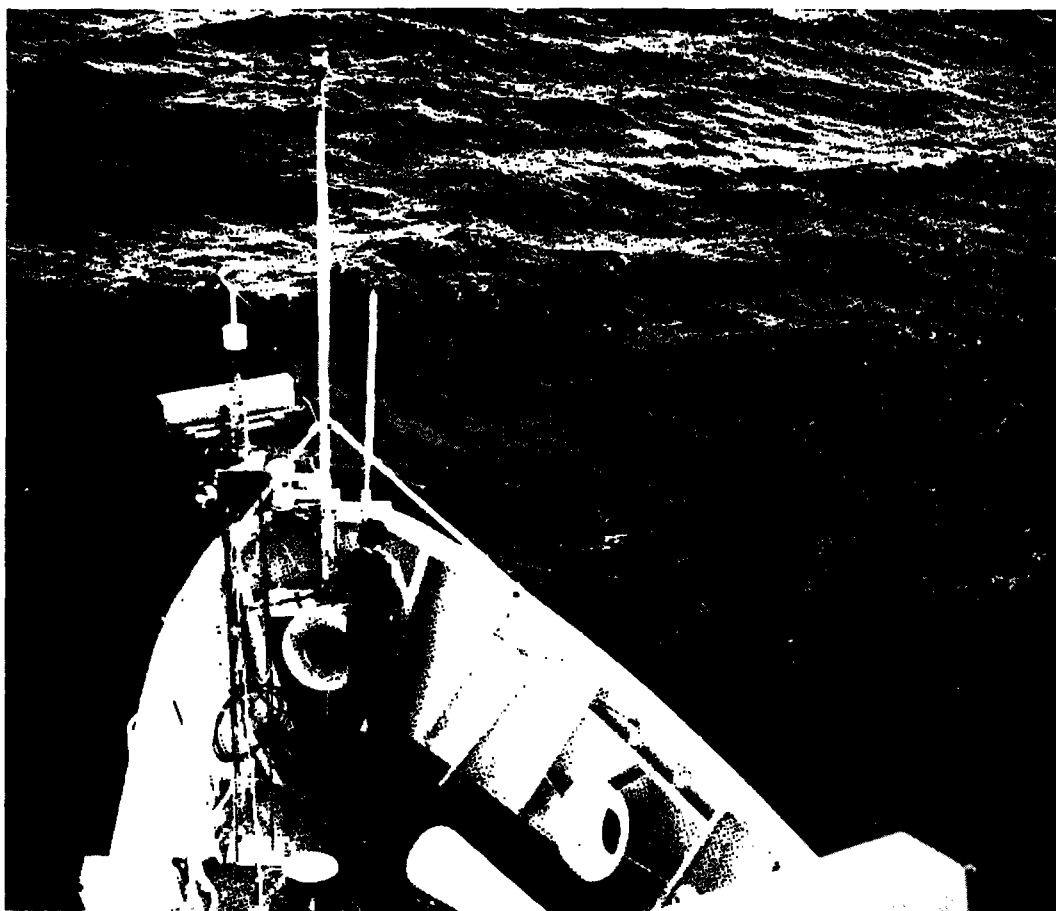


Fig. 7 — View of bow, showing location of forward particle counter

In Fig. 13 and in the rest of the cases, a bow wind prevailed. This figure shows three distributions obtained during an encounter with a fog bank off the coast of Nova Scotia. The circles indicate the aerosol content outside of the fog region. The plus signs show a general increase in count, over the entire range of particles, as we approached the edge of the fog. The squares give an excellent example of a multimodal distribution inside the fog.

Another point of interest observed inside the fog, as well as elsewhere, is the variation in particle density with height, as seen in Fig. 14; this figure represents the same fog distribution as Fig. 13, but plots the results of the high-volume probes and the active probe. The difference in the large-size region could exist for several reasons. The relative wind velocity was low, and there could thus be some evaporation due to the warm hulk of the ship. On the other hand, the fog may really have had a vertical variation in particle count in that size region. The lack of fog events prevented any firm conclusions.

However, in other than fog conditions a vertical variation was observed with sufficient regularity and under enough conditions that some conclusions can be drawn from the set of

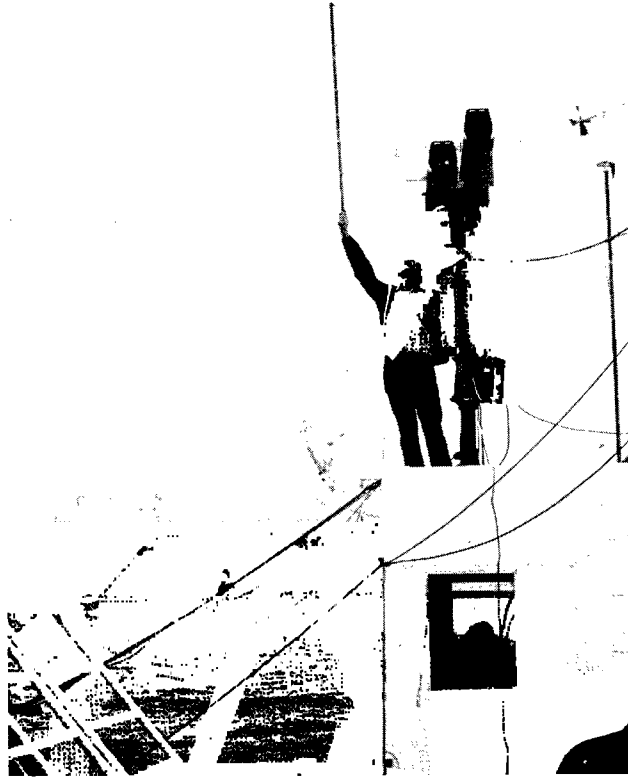


Fig. 8 — Checking airflow at the entrance to the particle counters

data. The data in Figs. 15a and 15b indicate that the magnitude of the vertical variation increases with windspeed for particle sizes more susceptible to fallout.

To get a perspective of the change in large particle count as a function of windspeed at a given level, we plotted the two 9-m results from the last example together in Fig. 16. The 15-m probe gave a similar but less pronounced effect.

MARITIME AEROSOL MODELS

Two measured distributions have been plotted in Fig. 17, which also shows the Shettle & Fenn Maritime Aerosol Distribution Model [3]. The latter calculates the aerosol extinction component in the LOWTRAN 3 computer code. In that code, the shape of the distribution is not varied; it is simply shifted up or down so that an extinction calculated in the green portion of the optical wavelength spectrum, $0.55 \mu\text{m}$, corresponds to the input visibility in the computer program.

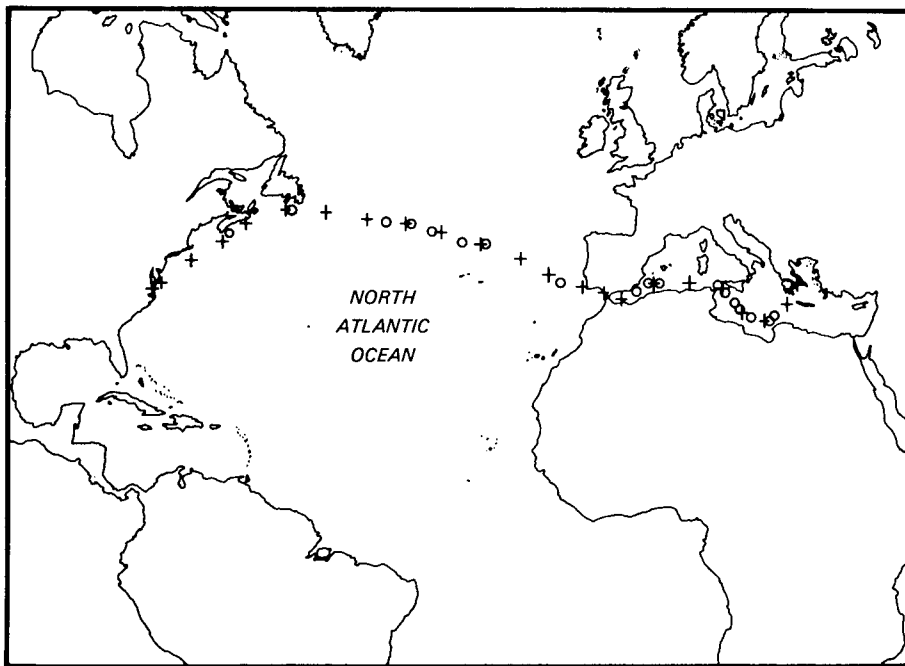


Fig. 9 — Ship's route



Fig. 10 — Ship's contribution to the marine atmosphere

Figure 17 shows, however, that the model does not fit either of the measured distributions by a vertical shift. Shettle & Fenn point out that we need a model with both windspeed and relative-humidity parameters. Wells et al. have a model [4] that includes these parameters; the data gathered on this cruise will be used to update and refine that model.

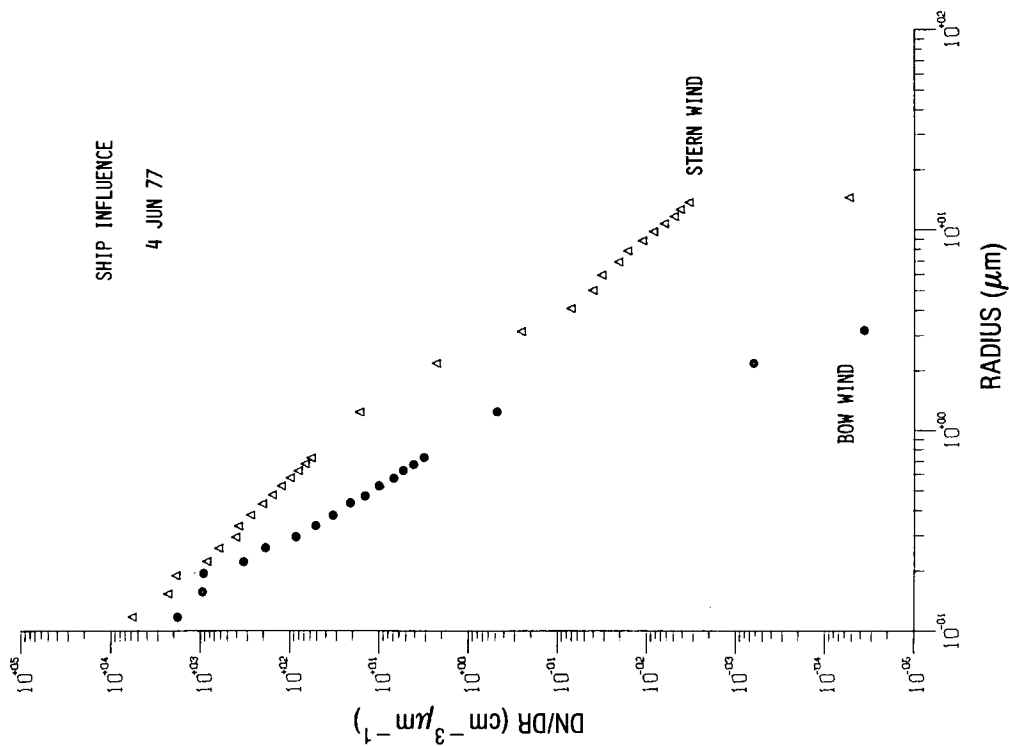


Fig. 11 — Comparison of distributions of marine and ship aerosols

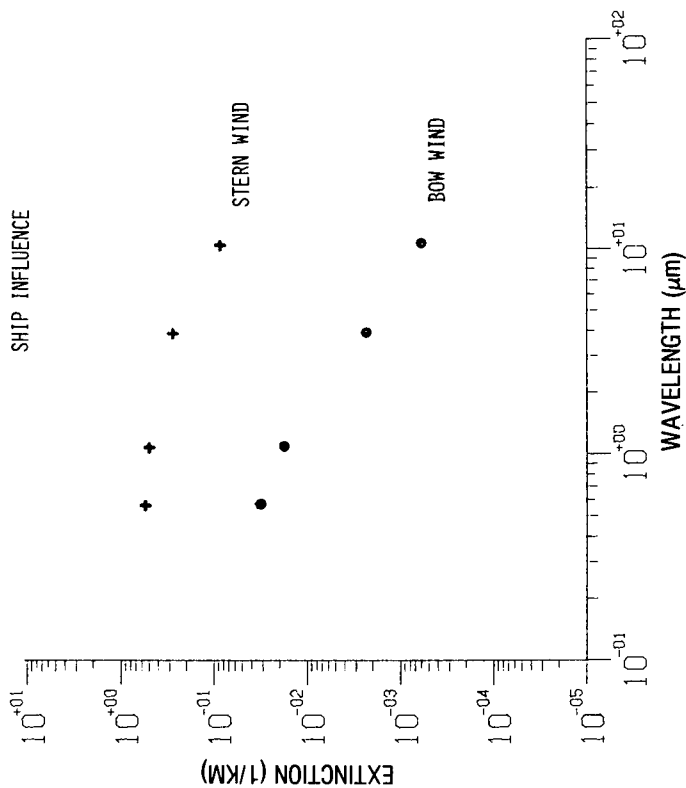


Fig. 12 — Computed extinction coefficients within and without the ship's influence (stern wind and bow wind, respectively)

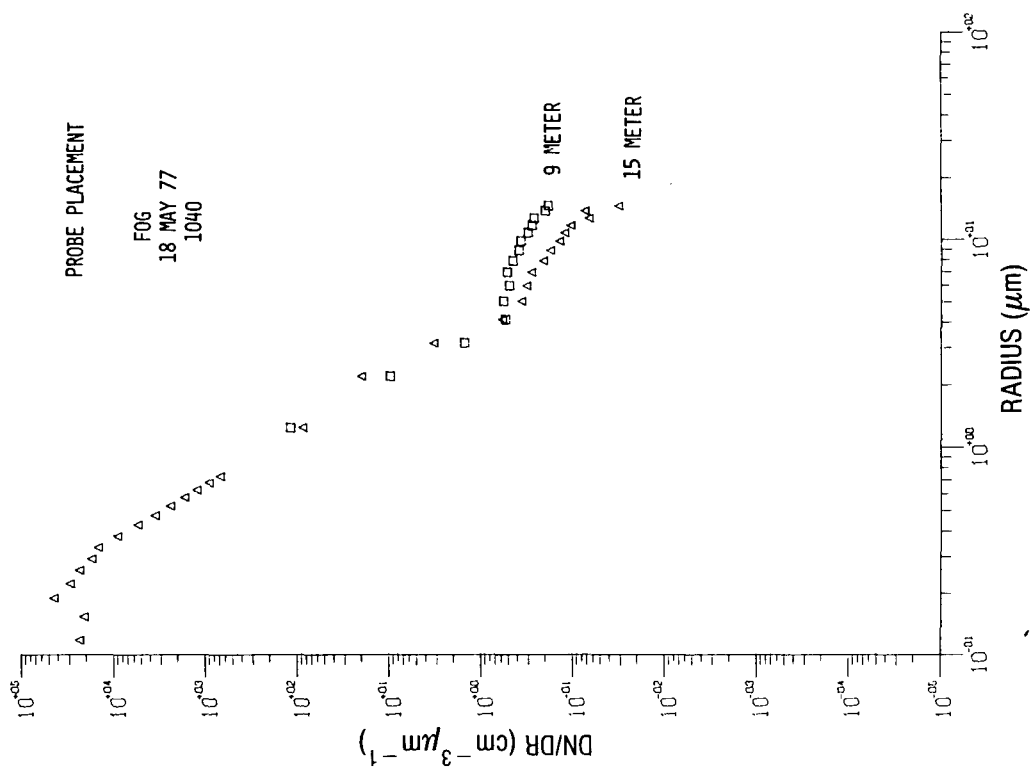


Fig. 14 — Fog size distributions at two heights above the surface

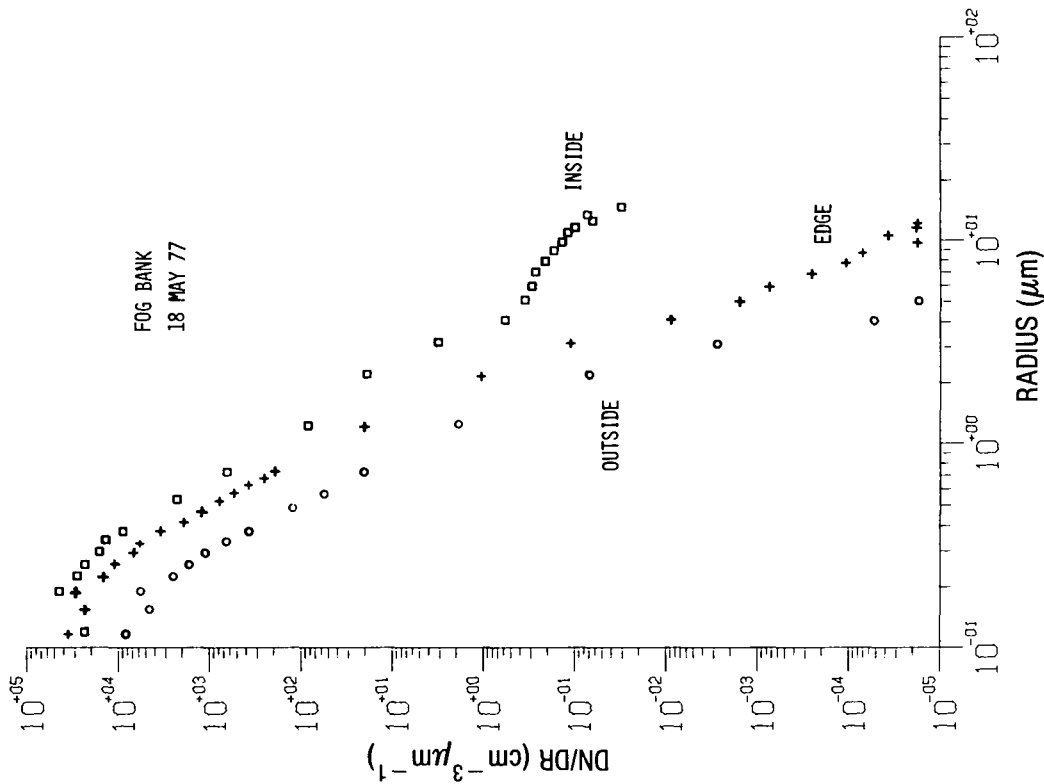


Fig. 13 — Aerosol size distributions in and around a fog bank

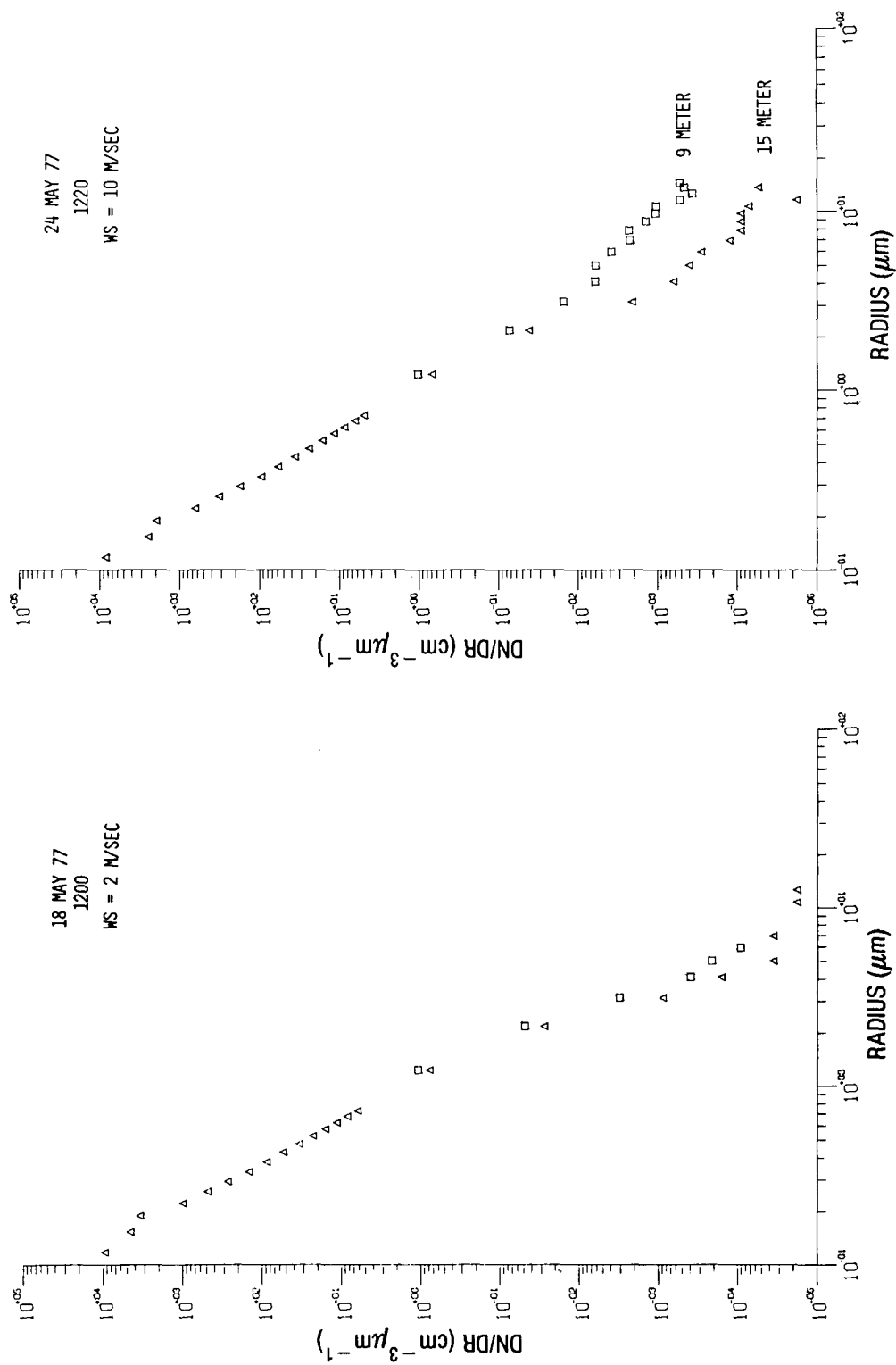


Fig. 15 — Influence of windspeed on size distributions at two heights

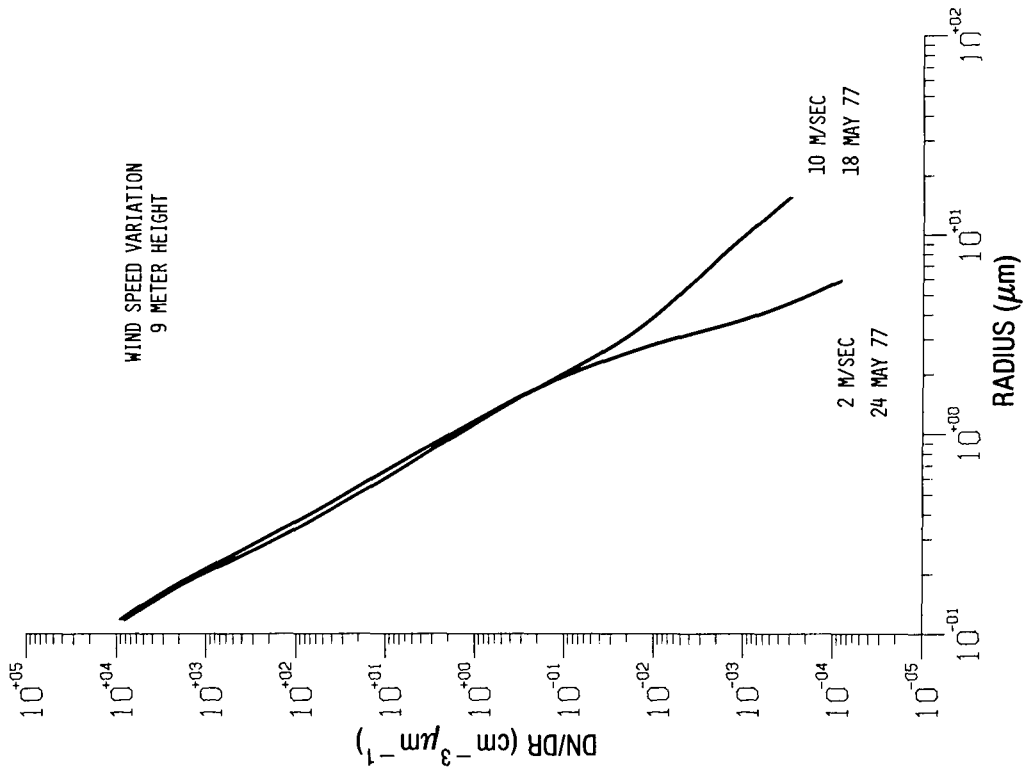
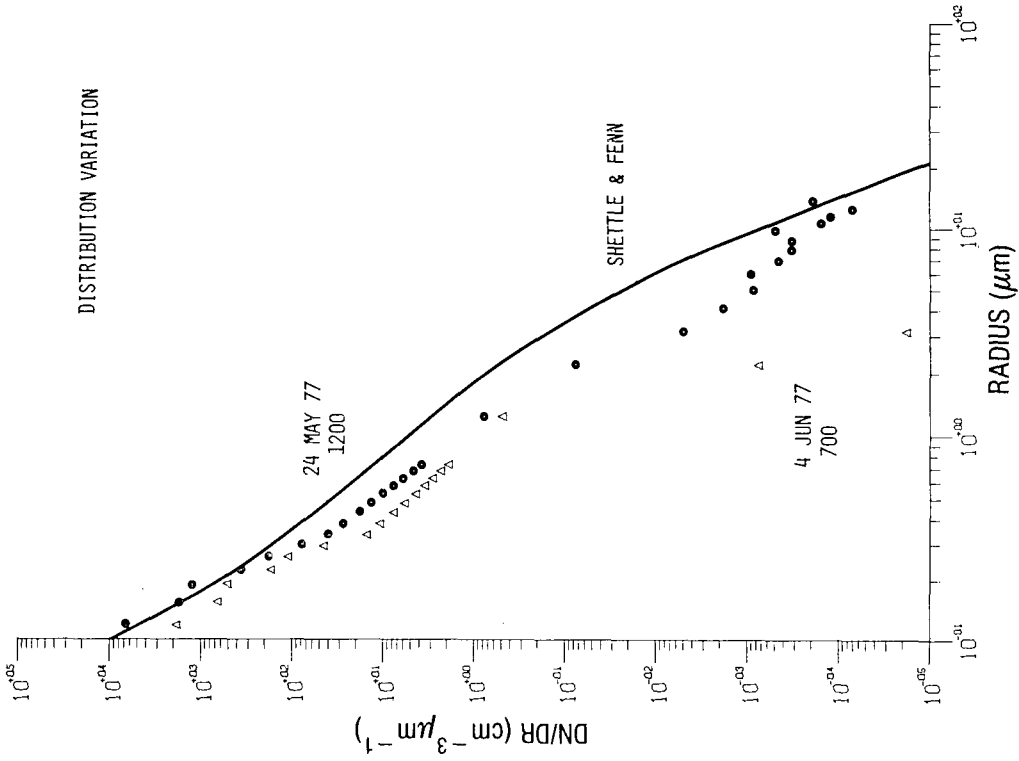


Fig. 17 — Atlantic and Mediterranean size distributions compared with predictions of Shettle and Fenn model

Fig. 16 — Comparison of size distributions at two windspeeds

Figure 18 presents the extinction coefficients calculated from the distributions in Fig. 17. One point of interest with respect to the two data samples is the difference in the ratios of the extinctions calculated at 0.55 μm . This reemphasizes that 10.6- μm extinction cannot generally be predicted from visibility measurements alone.

COMPUTATIONAL APPROACH

The equation used for calculating extinction coefficients from the aerosol size distributions is

$$\sigma_{\lambda,\eta} = \int_r Q(\lambda,\eta) \frac{dN(R)}{dR} \pi R^2 dR, \quad (1)$$

where σ is the extinction coefficient, Q is the Mie theory scattering efficiency factor, R is the particle radius, and dN/dR is the size distribution as shown in the examples above. The extinction coefficient is a function of both wavelength λ and index of refraction of the particles η . These calculations assume that the particles are spherical and that the index of refraction is known and remains constant over the particles size range. Because most of these data were gathered under conditions of high humidity (near 80% RH), both assumptions appear reasonable.

For sampling simplification purposes, an important point is the relative effect that particles of different sizes have on the extinction of a given wavelength. To observe this, rewrite Eq. (1) as

$$\sigma = \int \frac{d\sigma}{dR} dR, \quad (2)$$

where $d\sigma/dR$ is the extinction-coefficient distribution function. Plots of $d\sigma/dR$ are a function of the radius in Fig. 19 for 0.55- and 10.6- μm wavelengths, along with the size distribution from which they came.

For the 0.55- μm case, the main contributors to extinction are the particles with radii between 0.2 and 1.0 μm . For this distribution, the extinction could be calculated accurately for the 0.55- μm wavelength by knowing size distribution only in the 0.2- to 1.0- μm radius region. Interestingly enough, for this distribution the same is true in the 10.6- μm wavelength case. Generally, we think of the larger particles as contributing the most to extinction of the infrared. However, this is only the case if there are large particles; there are effectively none in this distribution.

Figure 20 shows a similar calculation for the fog encounter. Once again, for the green, the primary contributors are the particles in the 0.2- to 1.0- μm radius region. For the 10.6- μm wavelength, however, both small and large particles contribute on a more nearly even basis. Specifically, since the $d\sigma/dR$ curve has not begun to drop in value at the upper particle limit, the total extinction-coefficient value of 1.10 km is invalid, since the integrand still contributes significantly to the value of the integral. The conclusions for this sample are twofold: small particles are important even for 10.6 μm , and a valid result requires extinction information about particles larger than those measured here (i.e., above 15 μm in radius).

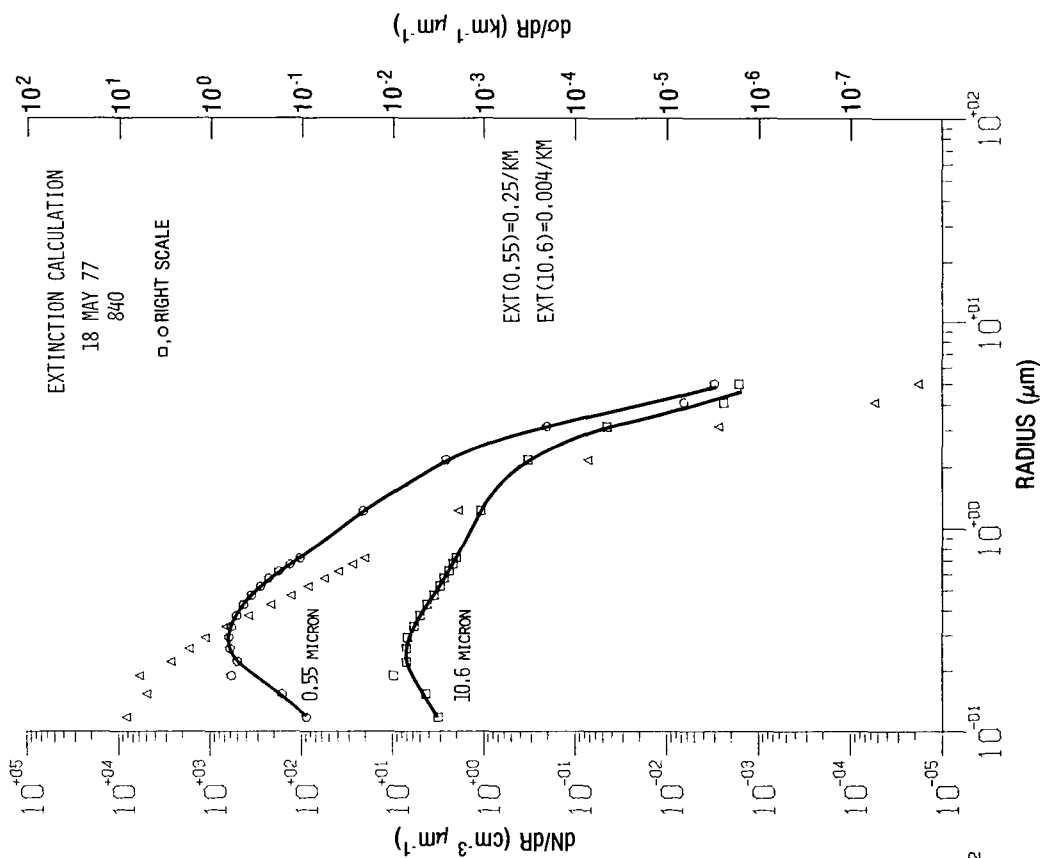


Fig. 19 — Extinction-coefficient calculation for a clear-air case

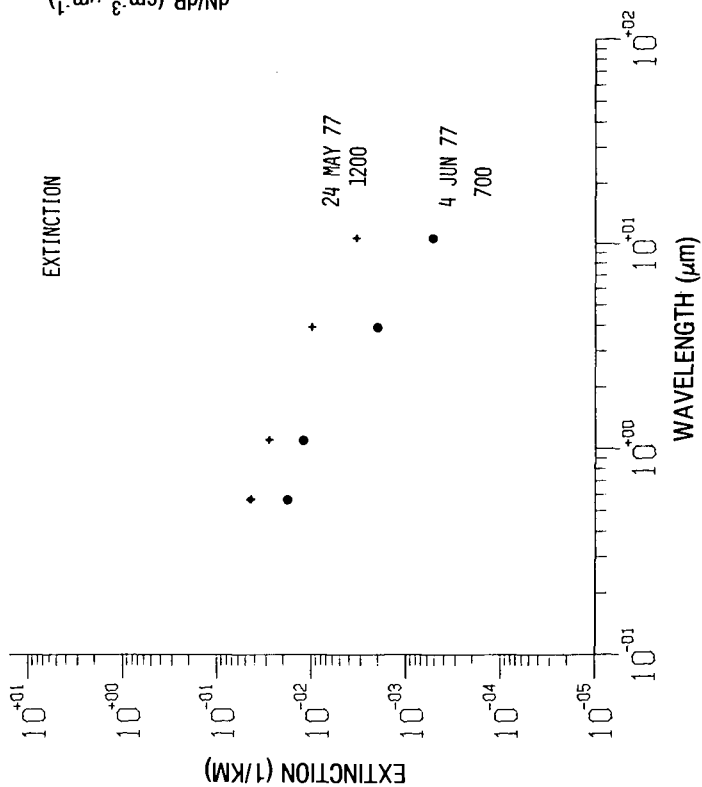


Fig. 18 — Computed extinction coefficients for the two samples in Fig. 17

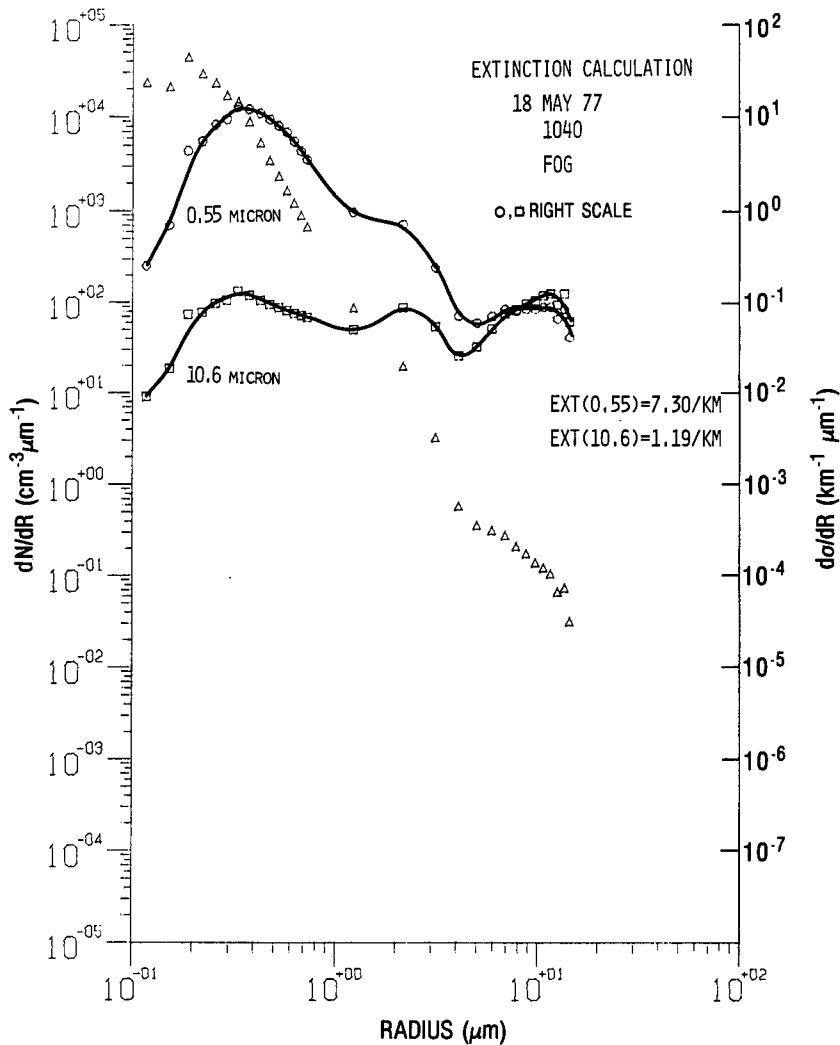


Fig. 20 — Extinction-coefficient calculation for fog

Note that for this last case, the high particle density would most likely require multiple scattering considerations to obtain the proper extinction value.

SUMMARY

We obtained aerosol size measurements at sea on the Atlantic and in the Mediterranean, under a limited variety of weather conditions. Results indicated that (a) extreme care must be taken to ensure that samples are of the marine atmosphere and not that of the ship; (b) for high wind conditions, there is a strong vertical variation in particle density for particles larger than 2.0 μm; (c) at a given height from the surface, these same size particles have a density that increases with windspeed; (d) the LOWTRAN 3 approach to aerosol extinction is inadequate without an improved maritime aerosol model (as suspected for some time); and (e) infrared extinction cannot be predicted from visibility measurements alone.

TRUSTY AND COSDEN

The size distribution in clear conditions was steeper than is usually associated with the "marine aerosol." In these conditions, accurate extinctions at $0.55\ \mu\text{m}$ could be obtained from particle information over a restricted size range of 0.2 to $1.0\ \mu\text{m}$. Extinction calculations at $10.6\ \mu\text{m}$ require expanded instrumentation, so that particles larger than $15\ \mu\text{m}$ can be added to the known size distribution, particularly in the presence of the many large particles of maritime fog.

REFERENCES

1. E.E. Hindman II, *Bull. Amer. Meteorol. Soc.* **58**, 592 (1977).
2. W.A. Hoppel, "Relationship between Dry Aerosol Size, Critical Supersaturation, and Size at High Relative Humidity," Preprints, American Meteorological Society, Conference on Cloud Physics and Atmospheric Electricity, Issaquah, Washington, Aug. 1978.
3. E.P. Shettle and R.W. Fenn, "Models of the Atmospheric Aerosols and Their Optical Properties," AGARD Conf. Proc. No. 183, *Optical Propagation in the Atmosphere*, p. 2.1-2.16, 1976. Presented at the Electromagnetic Wave Propagation Panel Symposium, Lyngby, Denmark, Oct. 27-31, 1975. (Available from NTIS, No. N76-29817.)
4. W.C. Wells, G. Gal, and M.W. Munn, *Appl. Opt.* **16**, 654 (1977).

Appendix

AEROSOL DATA

As examples of marine atmosphere aerosol data, we have listed the 20-min averages of measurements that we made during the times the ship was stopped and turned into the wind. Table A1 gives the particle density distribution $dN/dR(\text{cm}^{-3} \mu\text{m}^{-1})$ as a function of the radius of the probe bin centers. For Probe 1 we give results from only the first seven bins. Due to a double-valued sensitivity in the detection response, the data for the larger size ranges of that probe have proven to be inconsistent in many instances. For the purpose of calculating extinction coefficients, we fit a line between the value for the seventh bin of Probe 1 (ASASP) and the first bin of Probe 2 (CSASP). For convenience, the radii chosen for the fitted line are the same as the remaining eight bin centers of Probe 1. The plotted curves in this report show the form of the resulting fit.

Table A2 gives meteorological parameters and, for four wavelengths, calculated extinction coefficients. (The extinction calculations do not include molecular absorption.)

We have listed the particle probe bin edges in Table A3 to aid those who may wish to put the aerosol data into a form different from the one we have chosen.

TRUSTY AND COSDEN

Table A1a—Twenty-minute Averages of dN/dR ($\text{cm}^{-3} \mu\text{m}^{-1}$) vs Radius (μm)

RADIUS	0.12	0.15	0.19	0.22	0.26	0.29	0.33	1.22	2.17	3.12	4.07	
22 MAY 77	1220	4.00E 03	7.71E 02	4.57E 02	1.17E 02	6.57E 01	5.71E 01	4.25E 01	6.95E-01	5.89E-03	2.53E-04	2.00E-04
	1240	4.29E 03	9.43E 02	5.71E 02	1.54E 02	9.43E 01	6.00E 01	3.75E 01	9.58E-01	1.47E-02	5.05E-04	1.05E-04
	1300	4.29E 03	1.09E 03	6.57E 02	1.57E 02	8.86E 01	6.57E 01	4.25E 01	7.79E-01	9.79E-03	5.16E-04	1.26E-04
	1720	2.74E 03	4.86E 02	3.14E 02	7.43E 01	5.71E 01	3.71E 01	1.87E 01	4.95E-01	1.05E-02	3.26E-04	1.47E-04
	1740	2.74E 03	5.43E 02	3.43E 02	8.29E 01	6.00E 01	2.74E 01	2.17E 01	5.37E-01	1.37E-02	5.58E-04	2.00E-04
	1800	2.86E 03	5.43E 02	3.71E 02	1.00E 02	6.29E 01	4.00E 01	2.75E 01	6.63E-01	1.26E-02	4.84E-04	1.79E-04
24 MAY 77	120	1.69E 03	2.60E 02	2.11E 02	6.86E 01	4.00E 01	2.06E 01	2.02E 01	2.84E-01	1.04E-02	4.63E-04	1.79E-04
	140	1.71E 03	2.43E 02	2.11E 02	8.29E 01	4.00E 01	3.14E 01	1.57E 01	2.95E-01	1.68E-02	6.21E-04	2.63E-04
	200	1.63E 03	2.17E 02	2.20E 02	7.43E 01	1.97E 01	2.83E 01	1.99E 01	1.47E-02	5.58E-04	2.63E-04	
	1220	8.57E 03	2.51E 03	1.97E 03	6.29E 02	3.14E 02	1.80E 02	9.50E 01	6.95E-01	4.11E-02	2.11E-03	6.21E-04
26 MAY 77	2100	1.97E 03	1.26E 03	1.31E 03	4.57E 02	2.80E 02	1.40E 02	8.50E 01	4.21E-01	8.63E-04	0.00E 00	0.00E 00
	2120	2.03E 03	1.34E 03	1.31E 03	4.86E 02	2.86E 02	1.29E 02	9.50E 01	4.11E-01	1.26E-03	7.16E-05	1.79E-05
	2140	1.97E 03	1.29E 03	1.31E 03	4.86E 02	2.37E 02	1.49E 02	9.75E 01	4.11E-01	1.37E-03	1.79E-05	0.00E 00
31 MAY 77	2120	1.40E 03	5.14E 02	3.71E 02	1.03E 02	6.57E 01	2.86E 01	1.65E 01	4.95E-01	1.02E-02	1.05E-04	7.16E-05
1 JUN 77	900	1.97E 03	1.31E 03	1.34E 03	4.86E 02	2.63E 02	1.43E 02	9.25E 01	1.16E 00	1.03E-02	2.53E-04	1.47E-04
	920	1.80E 03	1.17E 03	1.17E 03	4.00E 02	2.11E 02	1.09E 02	7.25E 01	1.16E 00	2.00E-02	4.84E-04	1.47E-04
	1400	1.17E 03	7.43E 02	8.57E 02	3.14E 02	1.66E 02	9.14E 01	3.75E 01	5.37E-01	7.05E-03	2.84E-04	1.47E-04
	1420	1.31E 03	8.29E 02	9.71E 02	3.43E 02	1.91E 02	9.43E 01	5.25E 01	4.42E-01	5.58E-03	8.95E-05	1.58E-04
	1440	1.34E 03	8.00E 02	8.29E 02	3.14E 02	1.60E 02	8.29E 01	5.25E 01	4.63E-01	4.53E-03	1.26E-04	7.16E-05
3 JUN 77	1200	6.29E 03	4.57E 03	4.00E 03	2.86E 03	1.83E 03	1.54E 02	6.25E 02	9.16E-01	1.89E-03	5.37E-05	1.79E-05
	1400	3.43E 03	2.34E 03	2.20E 03	8.86E 02	4.86E 02	2.54E 02	1.55E 02	7.68E-01	3.89E-01	1.05E-04	3.58E-05
	1420	3.14E 03	2.20E 03	2.00E 03	7.14E 02	4.00E 02	1.94E 02	1.12E 02	7.58E-01	2.63E-03	1.26E-04	5.37E-05
	1440	2.86E 03	2.11E 03	1.94E 03	6.29E 02	3.14E 02	1.89E 02	1.03E 02	8.63E-01	5.26E-03	1.47E-04	1.47E-04
	2120	2.40E 03	1.60E 03	1.49E 03	5.14E 02	2.71E 02	1.54E 02	9.00E 01	8.63E-01	5.89E-03	1.05E-04	3.58E-05
	2140	2.34E 03	1.51E 03	1.49E 03	5.43E 02	3.43E 02	1.57E 02	1.07E 02	9.47E-01	7.58E-03	1.47E-04	3.58E-05
	2200	2.66E 03	1.86E 03	1.80E 03	6.57E 02	3.71E 02	2.00E 02	1.10E 02	9.16E-01	4.21E-03	7.16E-05	0.00E 00
4 JUN 77	620	1.80E 03	9.14E 02	8.86E 02	3.43E 02	1.86E 02	8.86E 01	5.25E 01	4.74E-01	6.21E-04	3.58E-05	0.00E 00
	640	1.74E 03	8.00E 02	8.00E 02	2.71E 02	1.54E 02	6.86E 01	4.50E 01	4.95E-01	6.42E-04	0.00E 00	0.00E 00
	700	1.83E 03	6.57E 02	5.14E 02	1.69E 02	1.09E 02	4.57E 01	1.50E 01	4.84E-01	7.47E-04	1.79E-05	0.00E 00
	820	2.17E 03	1.09E 03	1.09E 03	3.71E 02	2.23E 02	1.31E 02	6.00E 01	7.89E-01	1.68E-02	5.58E-04	2.84E-04
	840	2.11E 03	1.29E 03	1.40E 03	5.43E 02	2.83E 02	1.66E 02	8.50E 01	9.58E-01	1.16E-02	2.84E-04	1.79E-04
	900	2.26E 03	1.40E 03	1.46E 03	5.43E 02	2.69E 02	1.57E 02	1.00E 02	9.58E-01	9.05E-03	2.00E-04	1.26E-04
5 JUN 77	20	1.06E 04	7.43E 03	6.00E 03	1.71E 03	7.71E 02	3.43E 02	1.90E 02	1.00E 00	9.16E-03	1.47E-04	5.37E-05
	40	6.86E 03	4.86E 03	4.00E 03	1.20E 03	5.14E 02	2.46E 02	1.32E 02	8.63E-01	1.16E-02	2.84E-04	1.47E-04
	100	4.86E 03	2.83E 03	2.29E 03	6.00E 02	3.14E 02	1.43E 02	8.75E 01	8.11E-01	1.05E-02	2.84E-04	1.26E-04
	440	5.43E 03	2.86E 03	2.46E 03	5.71E 02	2.71E 02	1.14E 02	5.75E 01	7.58E-01	1.47E-02	5.37E-04	2.11E-04
	500	5.71E 03	3.43E 03	2.69E 03	6.29E 02	2.54E 02	1.20E 02	7.00E 01	7.05E-01	1.04E-02	3.37E-04	2.00E-04
	820	8.00E 03	5.14E 03	4.00E 03	9.71E 02	3.71E 02	1.86E 02	8.75E 01	7.37E-01	9.89E-03	2.00E-04	8.95E-05
	840	7.43E 03	4.57E 03	3.71E 03	8.57E 02	3.71E 02	1.60E 02	1.00E 02	7.26E-01	3.37E-03	5.37E-05	0.00E 00
	900	7.43E 03	4.57E 03	3.43E 03	8.29E 02	3.14E 02	1.37E 02	7.50E 01	6.42E-01	5.05E-03	7.16E-05	0.00E 00
	1420	7.43E 03	4.00E 03	3.14E 03	6.86E 02	2.80E 02	1.09E 02	6.00E 01	7.79E-01	1.37E-02	2.00E-04	1.79E-04
	1440	7.71E 03	5.43E 03	4.29E 03	1.09E 03	4.29E 02	1.89E 02	9.75E 01	8.95E-01	9.68E-03	2.84E-04	3.58E-05
	1500	8.57E 03	6.00E 03	4.86E 03	1.14E 03	5.14E 02	2.03E 02	1.12E 02	8.74E-01	2.74E-03	1.79E-05	3.58E-05
	2200	6.86E 03	4.29E 03	3.43E 03	8.00E 02	3.14E 02	1.34E 02	6.12E 01	4.84E-01	4.84E-03	1.05E-04	0.00E 00
	2220	7.14E 03	3.14E 03	2.09E 03	4.57E 02	1.71E 02	7.71E 01	4.25E 01	3.95E-01	8.42E-03	3.37E-04	1.05E-04
	2240	7.14E 03	2.83E 03	1.97E 03	4.29E 02	1.60E 02	6.57E 01	3.75E 01	2.63E-01	7.89E-03	2.32E-04	5.37E-05

Table Alb-Twenty-minute Averages of dN/dR (cm⁻³ μm⁻¹) vs Radius (μm)

RADIUS	5.02	5.97	6.92	7.87	8.82	9.77	10.72	11.67	12.62	13.57	14.52
22 MAY 77	1220	3.58E-04	2.84E-04	8.95E-05	1.79E-04	1.05E-04	7.16E-05	7.16E-05	5.37E-05	7.16E-05	0.00E 00
	1240	1.58E-04	1.47E-04	8.95E-05	7.16E-05	1.26E-04	7.16E-05	7.16E-05	7.16E-05	7.16E-05	0.00E 00
	1300	3.58E-05	2.32E-04	8.95E-05	5.37E-05	8.95E-05	0.00E 00	5.37E-05	1.79E-05	7.16E-05	0.00E 00
	1720	1.58E-04	1.47E-04	1.58E-04	1.05E-04	7.16E-05	7.16E-05	0.00E 00	3.58E-05	3.58E-05	0.00E 00
	1740	1.26E-04	1.26E-04	1.58E-04	1.47E-04	1.79E-05	5.37E-05	7.16E-05	0.00E 00	3.58E-05	0.00E 00
	1800	1.58E-04	1.47E-04	7.16E-05	8.95E-05	1.47E-04	1.79E-05	7.16E-05	1.05E-04	1.47E-04	0.00E 00
24 MAY 77	120	0.00E 00	8.95E-05	3.58E-05	7.16E-05	1.79E-05	1.79E-05	3.58E-05	0.00E 00	1.79E-05	0.00E 00
	140	8.95E-05	8.95E-05	5.37E-05	3.58E-05	0.00E 00	0.00E 00	0.00E 00	1.79E-05	0.00E 00	0.00E 00
	200	1.05E-04	5.37E-05	3.58E-05	3.58E-05	1.79E-05	3.58E-05	0.00E 00	0.00E 00	0.00E 00	0.00E 00
	1220	4.11E-04	2.84E-04	1.26E-04	8.95E-05	8.95E-05	7.16E-05	1.79E-05	0.00E 00	5.37E-05	0.00E 00
26 MAY 77	2100	0.00E 00									
	2120	0.00E 00									
	2140	0.00E 00									
31 MAY 77	2120	7.16E-05	0.00E 00	0.00E 00	5.37E-05	3.58E-05	1.79E-05	3.58E-05	0.00E 00	1.79E-05	0.00E 00
1 JUN 77	900	5.37E-05	1.05E-04	1.58E-04	1.26E-04	3.58E-05	7.16E-05	3.58E-05	1.79E-05	1.79E-05	0.00E 00
	920	2.32E-04	2.00E-04	5.37E-05	5.37E-05	1.05E-04	5.37E-05	1.26E-04	7.16E-05	5.37E-05	0.00E 00
	1400	1.05E-04	7.16E-05	1.05E-04	1.79E-05	5.58E-05	3.58E-05	3.58E-05	3.58E-05	0.00E 00	0.00E 00
	1420	1.05E-04	1.05E-04	1.05E-04	3.58E-05	5.37E-05	1.79E-05	0.00E 00	0.00E 00	0.00E 00	0.00E 00
	1440	1.47E-04	8.95E-05	8.95E-05	5.37E-05	3.58E-05	0.00E 00				
3 JUN 77	1200	1.79E-05	1.79E-05	0.00E 00	1.79E-05	3.58E-05	0.00E 00				
	1400	7.16E-05	1.05E-04	5.37E-05	7.16E-05	5.37E-05	7.16E-05	3.58E-05	3.58E-05	5.37E-05	0.00E 00
	1420	1.79E-05	1.79E-05	1.79E-05	5.37E-05	3.58E-05	0.00E 00	3.58E-05	1.79E-05	1.79E-05	0.00E 00
	1440	3.58E-05	1.79E-05	1.26E-04	7.16E-05	1.05E-04	5.37E-05	3.58E-05	3.58E-05	1.79E-05	0.00E 00
	2120	3.58E-05	3.58E-05	0.00E 00	3.58E-05	3.58E-05	0.00E 00				
	2140	0.00E 00	0.00E 00	1.79E-05	1.79E-05	0.00E 00	1.79E-05	0.00E 00	1.79E-05	0.00E 00	0.00E 00
	2200	0.00E 00	0.00E 00	3.58E-05	0.00E 00	1.79E-05	0.00E 00				
4 JUN 77	620	0.00E 00									
	640	0.00E 00									
	700	0.00E 00									
	820	8.95E-05	2.11E-04	7.16E-05	1.26E-04	1.79E-04	1.79E-05	5.37E-05	7.16E-05	0.00E 00	0.00E 00
	840	1.79E-05	8.95E-05	3.58E-05	5.37E-05	7.16E-05	1.79E-05	5.37E-05	1.79E-05	5.37E-05	0.00E 00
	900	5.37E-05	3.58E-05	1.79E-05	5.37E-05	0.00E 00	3.58E-05	0.00E 00	1.79E-05	3.58E-05	0.00E 00
5 JUN 77	20	5.37E-05	0.00E 00	1.79E-05	7.16E-05	5.37E-05	3.58E-05	0.00E 00	5.37E-05	0.00E 00	0.00E 00
	40	1.79E-04	1.26E-04	1.26E-04	5.37E-05	5.37E-05	3.58E-05	5.37E-05	5.37E-05	0.00E 00	0.00E 00
	100	1.26E-04	7.16E-05	3.58E-05	7.16E-05	7.16E-05	5.37E-05	8.95E-05	3.58E-05	5.37E-05	0.00E 00
	440	1.58E-04	1.05E-04	8.95E-05	8.95E-05	5.37E-05	8.95E-05	3.58E-05	3.58E-05	3.58E-05	0.00E 00
	500	7.16E-05	3.58E-05	3.58E-05	3.58E-05	3.58E-05	5.37E-05	5.37E-05	5.37E-05	3.58E-05	0.00E 00
	820	1.05E-04	3.58E-05	7.16E-05	0.00E 00	5.37E-05	3.58E-05	1.79E-05	0.00E 00	5.37E-05	0.00E 00
	840	3.58E-05	0.00E 00	1.79E-05	1.79E-05	0.00E 00	0.00E 00	0.00E 00	1.79E-05	0.00E 00	0.00E 00
	900	5.37E-05	0.00E 00	0.00E 00	7.16E-05	0.00E 00					
	1420	5.37E-05	1.79E-05	0.00E 00	1.79E-05	1.79E-05	1.79E-05	0.00E 00	0.00E 00	0.00E 00	0.00E 00
	1440	7.16E-05	0.00E 00	5.37E-05	3.58E-05	0.00E 00	1.79E-05	5.37E-05	3.58E-05	1.79E-05	0.00E 00
	1500	1.79E-05	3.58E-05	3.58E-05	0.00E 00	0.00E 00	0.00E 00	1.79E-05	0.00E 00	0.00E 00	0.00E 00
	2200	0.00E 00	0.00E 00	7.16E-05	0.00E 00	3.58E-05	0.00E 00	1.79E-05	0.00E 00	0.00E 00	0.00E 00
	2220	8.95E-05	7.16E-05	1.79E-05	0.00E 00	5.37E-05	1.79E-05	5.37E-05	1.79E-05	0.00E 00	0.00E 00
	2240	3.58E-05	5.37E-05	3.58E-05	3.58E-05	0.00E 00	0.00E 00	0.00E 00	1.79E-05	0.00E 00	0.00E 00

TRUSTY AND COSDEN

Table A2—Twenty-minute Averages of Measured and Calculated Parameters

	AT	DP	WS	WD	WVP	RH	NUM	VOL	0.55	1.06	3.80	10.0	
22 MAY 77	1220	10.0	1.7	9.50	210.	5.20	56.0	198.	14.1	0.029	0.020	0.0041	0.0014
	1240	9.8	1.7	9.50	210.	5.20	57.0	221.	16.6	0.033	0.025	0.0054	0.0015
	1300	9.7	0.6	9.50	200.	4.80	53.0	229.	14.2	0.032	0.022	0.0043	0.0012
	1720	10.0	1.3	8.00	190.	5.00	53.0	133.	9.4	0.018	0.013	0.0031	0.0009
	1740	11.0	1.7	8.50	190.	5.20	54.0	137.	9.9	0.019	0.015	0.0033	0.0009
	1800	10.0	3.0	8.50	200.	5.70	61.0	144.	14.1	0.023	0.018	0.0042	0.0015
24 MAY 77	120	15.0	13.0	3.90	270.	11.00	88.0	83.	5.7	0.013	0.009	0.0019	0.0005
	140	15.0	13.0	3.45	270.	11.00	88.0	84.	5.6	0.013	0.009	0.0021	0.0005
	200	15.0	13.0	3.50	260.	11.00	88.0	81.	5.8	0.014	0.009	0.0021	0.0005
	1220	17.0	14.0	10.50	250.	12.00	85.0	509.	21.9	0.059	0.029	0.0058	0.0018
26 MAY 77	2100	16.0	11.0	3.45	140.	10.00	73.0	200.	11.1	0.040	0.019	0.0022	0.0007
	2120	16.0	12.0	3.80	140.	10.00	74.0	207.	11.4	0.042	0.019	0.0022	0.0007
	2140	16.0	11.0	3.85	140.	10.00	74.0	202.	11.4	0.042	0.019	0.0022	0.0007
31 MAY 77	2120	18.0	12.0	7.50	280.	10.00	69.0	90.	7.5	0.017	0.013	0.0027	0.0006
1 JUN 77	900	18.0	14.0	8.50	190.	12.00	76.0	207.	20.4	0.057	0.036	0.0060	0.0016
	920	18.0	14.0	8.00	180.	12.00	75.0	182.	20.8	0.050	0.034	0.0065	0.0018
	1400	19.0	11.0	2.10	280.	10.00	61.0	123.	10.6	0.028	0.017	0.0030	0.0009
	1420	19.0	11.0	4.75	220.	10.00	62.0	138.	10.0	0.030	0.016	0.0025	0.0008
	1440	19.0	11.0	4.75	190.	10.00	63.0	131.	9.6	0.029	0.016	0.0025	0.0007
3 JUN 77	1200	19.0	20.0	7.00	190.	18.00	100.0	854.	49.1	0.209	0.076	0.0062	0.0030
	1400	19.0	15.0	10.50	180.	13.00	82.0	355.	22.2	0.073	0.034	0.0044	0.0017
	1420	18.0	15.0	10.50	180.	13.00	80.0	318.	18.5	0.061	0.030	0.0040	0.0013
	1440	19.0	15.0	10.50	180.	13.00	81.0	296.	19.8	0.060	0.032	0.0047	0.0015
	2120	19.0	15.0	9.00	170.	13.00	78.0	238.	16.7	0.052	0.030	0.0044	0.0012
	2140	19.0	15.0	8.50	170.	13.00	80.0	239.	18.1	0.058	0.033	0.0048	0.0012
	2200	19.0	15.0	9.50	170.	13.00	80.0	279.	18.6	0.062	0.033	0.0046	0.0012
4 JUN 77	620	19.0	15.0	9.00	130.	13.00	77.0	155.	9.3	0.031	0.017	0.0023	0.0006
	640	19.0	15.0	9.00	130.	13.00	76.0	141.	8.8	0.028	0.016	0.0023	0.0006
	700	19.0	15.0	9.00	120.	13.00	75.0	119.	6.7	0.018	0.012	0.0021	0.0005
	820	19.0	15.0	6.00	230.	12.00	74.0	187.	16.4	0.041	0.025	0.0048	0.0014
	840	19.0	15.0	6.50	190.	13.00	77.0	215.	19.0	0.053	0.032	0.0053	0.0015
	900	19.0	15.0	7.50	180.	13.00	77.0	227.	18.3	0.056	0.033	0.0050	0.0013
5 JUN 77	20	19.0	14.0	10.50	180.	12.00	73.0	963.	35.3	0.117	0.047	0.0058	0.0023
	40	19.0	14.0	10.50	180.	12.00	70.0	636.	27.0	0.084	0.037	0.0052	0.0019
	100	19.0	14.0	9.50	190.	12.00	71.0	399.	20.6	0.057	0.029	0.0047	0.0016
	440	19.0	14.0	6.50	190.	12.00	73.0	418.	19.0	0.050	0.026	0.0046	0.0015
	500	19.0	14.0	6.50	190.	12.00	72.0	459.	19.3	0.053	0.026	0.0042	0.0015
	820	20.0	14.0	7.00	180.	12.00	72.0	666.	23.2	0.069	0.030	0.0043	0.0016
	840	20.0	14.0	7.00	180.	12.00	72.0	612.	21.2	0.068	0.030	0.0038	0.0014
	900	20.0	14.0	7.00	170.	12.00	69.0	595.	19.0	0.059	0.025	0.0034	0.0012
	1420	20.0	15.0	7.50	130.	13.00	72.0	557.	19.6	0.056	0.027	0.0044	0.0014
	1440	20.0	15.0	8.00	150.	13.00	73.0	684.	25.3	0.077	0.034	0.0049	0.0017
	1500	20.0	15.0	8.00	140.	13.00	73.0	761.	26.0	0.084	0.036	0.0045	0.0017
	2200	20.0	15.0	7.50	140.	12.00	72.0	563.	17.2	0.054	0.022	0.0028	0.0011
	2220	20.0	14.0	7.00	140.	12.00	70.0	463.	12.5	0.035	0.014	0.0021	0.0009
	2240	20.0	14.0	7.00	140.	12.00	71.0	446.	10.9	0.032	0.012	0.0018	0.0007

Table A3 — Bin-Edge Locations
for Probes in Table A1

Particle Radius (μm)	
ASASP Probe 1	CSASP Probe 2
0.1	0.75
0.135	1.7
0.17	2.65
0.205	3.6
0.24	4.55
0.275	5.5
0.31	6.45
0.35	7.4
0.4	8.35
0.45	9.3
0.5	10.25
0.55	11.2
0.6	12.15
0.65	13.1
0.7	14.05
0.75	15.0